



HAL
open science

Dymeclin, the gene underlying Dyggve-Melchior-Clausen syndrome, encodes a protein integral to extracellular matrix and Golgi organisation and is associated with protein secretion pathways critical in bone development.

Celine Denais, Carolyn Dent, Laura Southgate, Jacqueline Hoyle, Dimitra Dafou, Richard Charles Trembath, Rajiv David Machado

► **To cite this version:**

Celine Denais, Carolyn Dent, Laura Southgate, Jacqueline Hoyle, Dimitra Dafou, et al.. Dymeclin, the gene underlying Dyggve-Melchior-Clausen syndrome, encodes a protein integral to extracellular matrix and Golgi organisation and is associated with protein secretion pathways critical in bone development.. Human Mutation, 2011, 32 (2), pp.231. 10.1002/humu.21413 . hal-00612011

HAL Id: hal-00612011

<https://hal.science/hal-00612011>

Submitted on 28 Jul 2011

HAL is a multi-disciplinary open access archive for the deposit and dissemination of scientific research documents, whether they are published or not. The documents may come from teaching and research institutions in France or abroad, or from public or private research centers.

L'archive ouverte pluridisciplinaire **HAL**, est destinée au dépôt et à la diffusion de documents scientifiques de niveau recherche, publiés ou non, émanant des établissements d'enseignement et de recherche français ou étrangers, des laboratoires publics ou privés.



Dymeclin, the gene underlying Dyggve-Melchior-Clausen syndrome, encodes a protein integral to extracellular matrix and Golgi organisation and is associated with protein secretion pathways critical in bone development.

Journal:	<i>Human Mutation</i>
Manuscript ID:	humu-2010-0467.R1
Wiley - Manuscript type:	Research Article
Date Submitted by the Author:	25-Oct-2010
Complete List of Authors:	Denais, Celine; King's College London, Medical and Molecular Genetics Dent, Carolyn; King's College London, Medical and Molecular Genetics Southgate, Laura; King's College London, Medical and Molecular Genetics Hoyle, Jacqueline; King's College London, Medical and Molecular Genetics Dafou, Dimitra; King's College London, Medical and Molecular Genetics Trembath, Richard; King's College London, Medical and Molecular Genetics Machado, Rajiv; King's College London, Medical and molecular genetics
Key Words:	Dymeclin, Skeletal dysplasia, secretion, chondrogenesis, Golgi

SCHOLARONE™
Manuscripts

1
2
3 **Title: Dymeclin, the gene underlying Dyggve-Melchior-Clausen syndrome, encodes**
4 **a protein integral to extracellular matrix and Golgi organisation and is associated**
5 **with protein secretion pathways critical in bone development.**
6
7
8

9
10 **Authors: Celine Denais¹, Carolyn L. Dent¹, Laura Southgate¹, Jacqueline Hoyle¹,**
11 **Dimitra Dafou¹, Richard C. Trembath^{1*}, Rajiv D. Machado¹.**
12
13
14

15
16
17 **Author's affiliations:**

18 ¹King's College London, Department of Medical & Molecular Genetics, School of
19 Medicine, Guy's Hospital, London, UK.
20
21
22

23
24
25 ***Corresponding author:**

26 Professor Richard C. Trembath, Professor of Medical Genetics, King's College London,
27 Department of Medical & Molecular Genetics, School of Medicine, Floor 8 Tower Wing,
28 Guy's Hospital, London SE1 9RT, United Kingdom. Tel: +44(0)2071887993; Fax:
29 +44(0)2071882585; Email: richard.trembath@kcl.ac.uk
30
31
32
33
34
35
36
37
38
39
40
41
42
43
44
45
46
47
48
49
50
51
52
53
54
55
56
57
58
59
60

ABSTRACT

Dyggve-Melchior-Clausen syndrome (DMC), a severe autosomal recessive skeletal disorder with mental retardation, is caused by mutation of the gene encoding Dymeclin. Employing patient fibroblasts with mutations characterized at the genomic and, for the first time, transcript level, we identified profound disruption of Golgi organization as a pathogenic feature, resolved by transfection of heterologous wild-type Dymeclin. Collagen targeting appeared defective in DMC cells leading to near complete absence of cell surface collagen fibres. DMC cells have an elevated apoptotic index ($p < 0.01$) likely due to a stress response contingent upon Golgi-related trafficking defects. We performed spatio-temporal mapping of Dymeclin expression in zebrafish embryos and identified high levels of transcript in brain and cartilage during early development. Finally, in a chondrocyte cDNA library, we identified two novel secretion pathway proteins as Dymeclin interacting partners, GOLM1 and PPIB. Together these data identify the role of Dymeclin in secretory pathways essential to endochondral bone formation during early development.

Deleted: The tightly regulated cleavage and secretion of the Golgi-associated protein GOLM1 by furin, a cycling protease, is severely dysregulated in DMC. PPIB null mutations lead to the skeletal dysplasia osteogenesis imperfecta, characterized by delayed export of pro-collagen to the Golgi apparatus.

KEY WORDS

Dymeclin, Skeletal dysplasia, secretion, chondrogenesis, Golgi.

INTRODUCTION

The osteochondroplasias are a heterogeneous group of skeletal disorders, the result of inherited defects in bone formation, growth and maintenance [Ortega et al., 2004; [Superti-Furga and Unger, 2007](#)]. To date, some 250 distinct clinical phenotypes have been reported with an incidence of 1 in 4000 across European populations [Stoll et al., 1989]. Dyggve-Melchior-Clausen syndrome (DMC) is part of a sub-group of osteochondroplasias known as the spondyloepimetaphyseal dysplasias (SEMDs) characterised by malformations of the vertebrae, with abnormal ossification of long bone epiphyses and metaphyses. DMC is a progressive SEMD with additional clinical features that include microcephaly, facial dysmorphism and variable mental retardation [Dyggve et al., 1962; Toledo et al., 1979; Beighton, 1990]. Classical radiological features of DMC include the appearance of lacy iliac crests, consistent with widespread bone abnormalities of development and growth [Spranger et al., 1975], driven by deficient chondrocyte organisation and differentiation with columnar structures that contain populations of degenerating cells [Horton and Scott, 1982; Nakamura et al., 1997].

DMC is a rare recessive disorder predominantly due to loss-of-function mutations in the *DYM* gene ([MIM ID: 607461](#)) located at chromosome 18q12 [Cohn et al., 2003; El Ghouzzi et al., 2003]. Defects in this gene also result in Smith-McCourt dysplasia (SMC), an allelic variant of DMC without mental retardation [Ehtesham et al., 2002; Cohn et al., 2003]. The ubiquitously expressed *DYM* transcript encodes Dymeclin, a novel 669 amino acid protein under tight evolutionary conservation, which does not belong to a recognised protein [family](#) and has limited characteristics for functional

Formatted: Font color: Orange

Deleted: network

1
2 motifs. Bioinformatic analyses predict the presence of an N-myristoylation site, several
3 transmembrane loops and dileucine motifs but, to date, these have not been
4 experimentally validated [Cohn et al., 2003; El Ghouzzi et al., 2003]. In short, the cellular
5 and molecular function of Dymeclin remains unclear, confounding efforts to better
6 elucidate the processes critical in the genesis of DMC and SMC.
7
8
9
10
11
12
13

Deleted: unambiguously

14 In the present study, the cellular functions of Dymeclin have been investigated by a
15 combinatorial approach. This report is the first to delineate, in human patient cell lines
16 characterised for Dymeclin loss-of-function mutations at the genomic and transcript
17 level, the profound consequences for Golgi and extracellular matrix organisation. Using a
18 zebrafish model, we demonstrate prominent head and cartilage *DYM* expression during
19 early development. By means of two yeast two-hybrid screens of protein-protein
20 interactions, we identified novel partners that provide insight into Dymeclin-associated
21 cellular function, likely to be critical for chondrocyte development and maintenance.
22 Together, these data reveal Dymeclin driven processes central to bone development
23 pathways, including Golgi organisation, Golgi-coupled protein secretion, and collagen
24 deposition in the extracellular matrix, thereby illuminating the likely molecular
25 mechanisms underlying DMC pathogenesis.
26
27
28
29
30
31
32
33
34
35
36
37
38
39
40

41 MATERIALS AND METHODS

42 Cell culture and transfection

43 Primary human wild-type (WT) fibroblasts were harvested from skin biopsies obtained
44 under ethics committee approval. All three mutant fibroblast lines were obtained from the
45
46
47
48
49
50
51
52
53
54
55
56
57
58
59
60

1
2 Coriell Institute (www.coriell.org), (Table 1). Primary lines, HeLa and U2OS cells were
3
4 cultured in Dulbecco's modified Eagle's medium with Glutamax (DMEM, GIBCO life
5 technologies) supplemented with 10% foetal bovine serum at 37 °C and 1%
6 penicillin/streptomycin. Transient transfections of HeLa and U2OS cells were performed
7
8 using Lipofectamine 2000 (Invitrogen) and FuGENE (Roche) respectively in accordance
9
10 with manufacturers' instructions.
11
12
13

14 15 16 17 **DNA, RNA isolation and RT-PCR**

18 DNA and total RNA was isolated from fibroblast cell lines and whole zebrafish embryos
19 using TRI Reagent (Sigma Aldrich) according to manufacturer's instructions. cDNA was
20 generated by priming with oligo dT using the First strand synthesis SuperScript II kit
21 (Invitrogen). Newly produced cDNA was used as a template in subsequent PCR reactions
22
23 to amplify regions of the *DYM* transcript ([Human: NM 017653.3](#), [Zebrafish:](#)
24 [NM 001002739.1](#)). All human and zebrafish genomic and cDNA primers are available
25 on request. Cycling conditions were as standard. [Identified mutations in DMC patient](#)
26 [samples were numbered at the nucleotide level on the basis that +1 corresponded to the A](#)
27 [of the ATG translation initiation codon in the reference sequence.](#)
28
29
30
31
32
33
34
35
36
37
38

39 **Quantitative PCR**

40 Quantitative PCR was carried out containing the TaqMan ABI 7700 with the ABI PRISM
41 Detection System using the Hs00214264_m1 assay which spans the *DYM* exon 8/9
42 junction (Applied Biosystems). Briefly, 2 µg of total RNA was reverse transcribed and
43 PCR performed according to manufacturer's instructions to a final volume of 20 µl. A
44
45
46
47
48
49
50
51
52
53
54
55
56
57
58
59
60

1
2
3
4
5
6
7
8
9
10
11
12
13
14
15
16
17
18
19
20
21
22
23
24
25
26
27
28
29
30
31
32
33
34
35
36
37
38
39
40
41
42
43
44
45
46
47
48
49
50
51
52
53
54
55
56
57
58
59
60

PCR reaction lacking the cDNA template was used as a control. The housekeeping gene, cyclophilin A (Hs99999904_m1) was used as an internal control. Each experiment was performed in triplicate. For data evaluation, resulting Ct values acquired in real-time qPCR for Dymeclin transcripts were normalized to the Ct values of cyclophilin A transcripts to yield the ΔCt value. Relative expression level (fold change) of Dymeclin in each experimental sample was calculated using $2^{-\Delta\Delta\text{Ct}}$ method where $\Delta\text{Ct} = \text{Ct (target gene)} - \text{Ct (reference gene)}$ and $\Delta\Delta\text{Ct} = \Delta\text{Ct (treated)} - \Delta\text{Ct (control)}$.

Yeast two-hybrid screen

The two bait constructs comprising Dymeclin amino acids 1-97 and 270-510 were generated by PCR amplification with full-length *DYM* cDNA as template and cloned into the yeast expression plasmid pGBDU-C1 [James et al., 1996]. The yeast strain PJ69-4a was sequentially transformed with the bait plasmid and chondrocyte library using the lithium acetate method devised by Agatep et al [Agatep et al., 1998]. The screen was performed by transforming yeast containing the bait plasmid, maintained on SD media lacking uracil, with 60 μg of DNA from the human chondrocyte library. Clones capable of interaction with the bait constructs were selected for by plating transformants on SD/-URA/-LEU/-HIS/ media supplemented with 1 mM 3-aminotriazole (3-AT). To estimate the strength of interaction the clones were subsequently streaked on to minimal media also lacking adenine. The bait plasmid was removed by growing the yeast on SD/-LEU supplemented with 1 g/L 5-fluoroorotic acid to select against plasmids encoding the uracil gene. Plasmids from the chondrocyte library were isolated using the Zymoprep kit (ZymoResearch) and transformed into the *E. coli* strain DH5 α . All library plasmid inserts

1
2 were sequenced using a primer to the Gal4 activation domain and identified using the
3
4 BLAST algorithm (www.ncbi.nlm.nih.gov/BLAST).
5
6
7

8 9 **GST pull-down assays**

10 To generate glutathione S-transferase (GST) fusion proteins, PPIB and GOLM1 were
11 cloned in frame to the 5' tag in the vector pGEX-4T1 (primers available on request). The
12 bacterial strain BL21 was freshly transformed with these constructs and single colonies
13 grown overnight. Expression of the fusion proteins were induced by the addition of 0.4
14 mM of isopropyl- β -D-thiogalactopyranoside (IPTG) for 3 h at 37 °C. Bacterial lysis was
15 achieved by sonication and the extracts were incubated with washed Glutathione-
16 Sepharose 4B beads (Amersham-Pharmacia). [³⁵S]methionine labelled full-length
17 Dymeclin was produced by *in vitro* translation using the TnT T7-coupled transcription
18 reticulocyte lysate system (Promega) following manufacturer's instructions. 20 μ l of the
19 translation reaction was added to purified GST fusion protein immobilised on the beads
20 along with 100 mM PMSF and protease inhibitor cocktail (Roche) at a 7 \times concentration.
21 The final volume was adjusted to 750 μ l with cold NETN buffer (0.5% Nonidet P-40, 1
22 mM EDTA, 20 mM Tris-HCl pH 8, 100 mM NaCl) and the mixture rotated for 90 min at
23 4 °C. After three washes in NETN buffer, proteins were dissociated from the beads by
24 incubation in 2 \times laemmli buffer and separated on a 10% SDS-PAGE gel. A 10% volume
25 of the labelled protein used in the GST pull-down was similarly resolved. Gels were
26 stained in Coomassie blue buffer and exposed to autoradiograph film for up to 5 days.
27
28
29
30
31
32
33
34
35
36
37
38
39
40
41
42
43
44
45

46 47 **Immunoprecipitation and immunoblotting**

48
49
50
51
52
53
54
55
56
57
58
59
60

1
2 Immunoprecipitation experiments were conducted on transiently transfected HeLa or
3 U2OS cells in 10 cm dishes. Cells were lysed in 1 ml lysis buffer (20 mM Tris-HCl pH
4 7.4, 150 mM NaCl, 2 mM CaCl₂, 1% Nonidet P-40, 5 mM EDTA and protease inhibitor
5 cocktail). Extracts were incubated overnight at 4 °C with either monoclonal antibody
6 against myc (Sigma Aldrich, clone 9E10) or anti-Flag antibody (Sigma Aldrich, F7425).
7 Protein A Sepharose CL 4B beads reconstituted as a 50% slurry (Amersham) were added
8 to the extracts and incubated for 2 h at 4 °C. Following 5 washes in lysis buffer, protein
9 was eluted into 2 × laemmli buffer and resolved by SDS-PAGE. Proteins were transferred
10 onto nitrocellulose and membranes were probed with myc or Flag antibodies diluted
11 1/500 in blocking buffer (5% milk powder, 0.1% Tween-20 in PBS). Secondary
12 antibodies were HRP conjugated and diluted according to manufacturer's instructions.
13 Proteins were detected by chemiluminescence using the EZ-ECL kit (GE Healthcare).
14
15
16
17
18
19
20
21
22
23
24
25
26
27
28

29 **Scanning laser confocal microscopy**

30
31 Prior to transfection, cells were plated on acid treated coverslips contained in 6-well
32 plates. Transfected cells were washed in PBS, fixed and permeabilised with absolute
33 methanol for 10 min at -20 °C. After blocking with PBS/1%BSA for 1 h at room
34 temperature cells were stained with primary antibodies diluted according to
35 manufacturer's instructions (anti-myc, Abcam, 9E10; anti-GFP, Santa Cruz, sc-8334;
36 Giantin, Abcam, 24586; PDI, Stressgen, SPA-891; anti-PPIB, Sigma Aldrich,
37 HPA012720). Anti-mouse Alexa 488 and anti-rabbit Alexa 555 were employed as
38 secondary antibodies. Before examination, coverslips were mounted with Vectashield
39 containing DAPI (Vector labs) to facilitate nuclear staining. Confocal microscopy was
40
41
42
43
44
45
46
47
48
49
50
51
52
53
54
55
56
57
58
59
60

1
2 performed on a Zeiss LSM510 laser scanning microscope (Zeiss, Thornwood, NY) using
3
4 a Zeiss 63 × 1.4 numerical aperture oil immersion lens.
5
6
7

8 **Electron microscopy**

9
10 Cells were plated onto acid-treated glass coverslips (13 mm in diameter) to a density of
11
12 0.5×10^5 in 24-well CellBIND Cell Culture Plates (Corning). After reaching sufficient
13
14 confluency, cells were processed for microscopy analysis by washing with $1 \times$ PBS
15
16 followed by fixation in 2.5% glutaraldehyde in 0.1 M sodium-cacodylate buffer, pH 7.4.
17
18 Samples were negatively stained with 1% uranyl acetate in water. Stained sections were
19
20 examined on a FEI Tecnai T12 BioTWIN transmission electron microscope and images
21
22 captured on a Gatan BioScan Model 792 MSC SI003 1 camera.
23
24
25
26

27 **Proliferation assay**

28
29 Cells to be tested were pelleted and CyQUANT GR dye/lysis buffer was added to each
30
31 cell pellet. A cell dilution series ranging from 100 to 50×10^4 cells was created in a 96-
32
33 well cell culture microplate (Corning) with CyQUANT GR dye/lysis buffer, in final
34
35 volumes of 200 μ l per well. A control 200 μ l well with no cells (CyQUANT GR dye/lysis
36
37 buffer only) was also prepared. The samples were incubated in darkness for 2 to 5 min at
38
39 room temperature. The fluorescence of each sample was measured with a CytoFluor 2350
40
41 fluorescence microplate reader, with 485 nm (± 10 nm) excitation and 530 nm (± 12.5 nm)
42
43 emission filters. For each experiment, a standard calibration curve was generated with
44
45 measured fluorescence values versus cell number, as determined from cell suspensions
46
47 using a haemocytometer (6-well culture plates of cells were harvested on days 1 to 8).
48
49
50
51
52
53
54
55
56
57
58
59
60

1
2 Sample fluorescence was measured as above, and growth curves were plotted as
3
4 fluorescence versus time.
5
6
7

8 **Apoptosis analysis**

9
10 Stress-induced apoptosis was quantified and differentiated from necrosis using the
11
12 Annexin-V-FLUOS direct fluorescence staining kit (Roche) according to the
13
14 manufacturer's instructions, which allows simultaneous staining of cell surface
15
16 phosphatidylserine (with Annexin-V-FLUOS) and necrotic cells (with propidium iodide).
17
18 Apoptotic cells were measured in mass cultures wherein cells were grown beyond the
19
20 stage of confluence to achieve stress-induced apoptosis [Tannock and Lee, 2001]. 1×10^6
21
22 cells were then washed with PBS, stained with Annexin V and Propidium Iodide for 15
23
24 min at room temperature and analysed using a Becton and Dickinson Aria II flow
25
26 cytometer. Experiments were performed in triplicate and a student t-test was used to
27
28 measure significance.
29
30
31
32

33 **Whole-mount *in situ* hybridisation**

34
35 Digoxigenin (DIG) labelled riboprobe was synthesised from plasmids harbouring full-
36
37 length zebrafish dymeclin using the DIG RNA labelling kit (Roche). *In situ* hybridisation
38
39 was performed as described previously [Jowett and Lettice, 1994]. Briefly,
40
41 prehybridisation, followed by probe hybridisation at 1/100 dilution was conducted at 68
42
43 °C overnight. The embryos were incubated with alkaline phosphatase-conjugated anti-
44
45 DIG antibody (Roche). The embryos were allowed to develop colour in nitro-blue
46
47 tetrazolium chloride and 5-bromo-4-chloro-3'-indolyphosphate-p-toluidine salt
48
49
50
51
52
53
54
55
56
57
58
59
60

1
2 (NBT/BCIP) (Roche) in developing buffer for 1.5 h. The embryos were photographed
3
4 with a Nikon FMZ microscope.
5
6
7

8 **RESULTS**

9 **Identification and characterisation of *DYM* mutations in patient cell lines**

10
11 DNA extracted from the three fibroblast lines (DMC10568, DMC02437 and DMC04997)
12
13 was screened for *DYM* mutations by direct sequencing. In DMC10568, a homozygous
14
15 single base pair deletion was identified within exon 10 (c.1004delT) predicting a
16
17 frameshift and the incorporation of an aberrant termination codon 65 amino acids
18
19 downstream (p.L335CfsX65). Homozygous acceptor splice site mutations were detected
20
21 in DMC02437 and DMC04997 in intron 10 (c.1126-1G>A) and intron 11 (c.1252-1G>A)
22
23 respectively (Fig. 1A). Sequence analysis of gel excised bands from patient cDNA
24
25 indicated complete skipping of exon 11 in DMC02437 resulting in an in-frame truncated
26
27 mRNA (Fig. 1B). Two major splice isoforms were identified in DMC04997, namely an
28
29 in-frame retention of the terminal 219 bases of intron 11, and a deletion of the first 28 bp
30
31 of exon 12 leading to a loss of frame (Fig. 1B). The gene defects identified in samples
32
33 DMC02437 and DMC04997 represent novel mutations. Quantitative RT-PCR confirms
34
35 the effect of all mutations to be a considerable reduction in levels of the Dymeclin
36
37 transcript (Fig. 1C).
38
39
40
41
42

43 **Dymeclin is localised to the Golgi apparatus and cytoplasm**

44
45 We sought to establish the distribution of Dymeclin in HeLa cells and the osteosarcoma
46
47 line U2OS using transiently transfected GFP-tagged constructs, due to the absence of a
48
49
50
51
52
53
54
55
56
57
58
59
60

1
2 reliable antibody against the native protein. Confocal microscopy revealed the presence
3 of Dymeclin in the cytosol but with marked focal concentrations. Co-staining with
4 Giantin, a marker of the cis-Golgi, demonstrated a high degree of co-localisation
5 indicating punctate enrichment of Dymeclin in the Golgi of both cell lines (Fig. 2A). By
6 contrast, no co-localisation was observed with PDI, a protein integral to the endoplasmic
7 reticulum (ER) (Fig. 2B).
8
9
10
11
12
13
14
15
16

17 **Phenotypic profiling of cells harbouring Dymeclin mutations**

18 Visualisation of Golgi and ER structure by confocal microscopy revealed significant
19 differences between WT and mutation-positive fibroblasts. In all three DMC lines, the
20 Golgi was markedly distended and disorganised by comparison to WT cells (Fig. 3A).
21 These changes to organelle structural conformation are unlikely to be due to impaired
22 cytoskeletal scaffolding as there was no demonstrable evidence of disruption to either the
23 microtubular or actin networks in mutant cells (data not shown). Notably, electron
24 micrographs of fibroblasts from DMC04997 illustrate that by contrast to the WT control,
25 DMC fibroblasts have a significantly lower density of collagen fibrils on the cell surface
26 (Fig. 3B). Measurement of the proliferative capacity of the three mutant cell cultures
27 revealed no significant differences to controls over a period of eight days (Fig. 3C). The
28 apoptotic cell population, measured by FACS analysis, was also unaltered under normal
29 culture conditions (data not shown). However, a significantly higher early apoptotic cell
30 population was observed for the mutants when stressed-induced apoptosis was achieved
31 by growing cells beyond the level of confluence (Fig. 3C).
32
33
34
35
36
37
38
39
40
41
42
43
44
45
46
47
48
49
50
51
52
53
54
55
56
57
58
59
60

1
2 Due to the marked perturbation of Golgi structure in Dymeclin deficient patient lines, we
3 sought to further interrogate the role of Dymeclin in regulating Golgi morphology. Over-
4 expression of WT Dymeclin in HeLa and U2OS lines resulted in substantive
5 condensation of the Golgi by comparison to cells transfected with GFP alone and
6 neighbouring untransfected cells (Fig. 4A). To exclude the possibility that the Golgi
7 compaction was due to transfection based toxicity mock transfections were used as a
8 control. To further corroborate these observations we next over-expressed wild-type
9 Dymeclin in mutant fibroblasts exhibiting grossly distended Golgi structures. Abnormal
10 Golgi were still evident upon the introduction of 0.5 μg of exogenous wild-type
11 Dymeclin. However, increasing the amount of transfected Dymeclin to 1 μg effectively
12 reversed abnormal Golgi conformation and positioning in mutant cells to a largely normal
13 phenotype (Fig. 4B). Taken together, these data indicate that the impact of Dymeclin loss
14 on sub-cellular morphology is a striking dysregulation of Golgi structure and impaired
15 deposition of extracellular collagen.
16
17
18
19
20
21
22
23
24
25
26
27
28
29
30
31
32

33 **Dymeclin expression during zebrafish embryonic development**

34 The temporal expression of the *dym* transcript was analysed in zebrafish embryos by RT-
35 PCR at different developmental time points ranging from the 32-cell stage and up to 48
36 hours post-fertilisation (hpf). Dymeclin was strongly expressed in early embryo
37 development but decreased dramatically by 48 hpf (Fig. 5A). As active zygotic
38 expression is considered to occur at the blastula stage these data signify that dymeclin is
39 highly expressed both maternally and zygotically. To examine the spatio-temporal
40 expression of the gene, whole mount *in situ* hybridisation in zebrafish was performed at
41
42
43
44
45
46
47
48
49
50
51
52
53
54
55
56
57
58
59
60

1
2
3 1, 2, 3 and 5 days post fertilisation (dpf). At all experimental time points studied, *dym*
4 staining was highly evident in the head region, specifically the fore-, mid- and hindbrain.
5
6 To better examine the developing jaw, the eyes were removed after 5 dpf. Dymeclin, at
7
8 this stage, was highly expressed in cartilaginous structures, in particular, the mandibular
9
10 arch otherwise referred to as Meckel's cartilages and in ceratobranchial arches (Fig. 5B).
11
12 These expression studies suggest a prominent role for dymeclin in brain and cartilage
13
14 formation at the earliest stages of embryonic development.
15
16

17 18 19 **Novel Dymeclin interacting partners identified by yeast two-hybrid screens**

20 To uncover Dymeclin-associated pathways of potential importance to bone development
21 and regulation, the Gal4 yeast two-hybrid system was used to screen a human
22 chondrocyte library using two bait constructs in independent experiments. Both baits
23
24 were confirmed as non-toxic and neither auto-activated the yeast auxotrophic reporter
25
26 genes. Each screen was conducted under high stringency conditions to select for the
27
28 strongest and most stable interactions. Of the putative protein partners identified in these
29
30 assays two were prioritised for further study, namely PPIB and GOLM1, identified as
31
32 binding the predicted N-terminal myristoylation domain and the conserved central region
33
34 of Dymeclin respectively. This approach yielded a novel set of protein interactions to
35
36 those previously described in the literature, yet the present findings complement and
37
38 expand on the emerging hypothesis that the wider Dymeclin network predominantly
39
40 comprises proteins with roles in ER-Golgi secretion and export [Osipovich et al., 2008].
41
42
43
44
45

46 47 ***In vitro* and *in vivo* validation of Dymeclin interacting proteins**

48
49
50
51
52
53
54
55
56
57
58
59
60

1
2 To substantiate the interaction between Dymeclin and proteins identified in the yeast two-
3 hybrid screen, GST pull-down assays were performed. Following incubation with GST-
4 tagged PPIB and GOLM1, ³⁵S radiolabelled full-length Dymeclin was successfully
5 recovered with each protein but not with GST alone, thereby validating physical
6 interaction (Fig. 6A). To investigate these interactions in a mammalian *in vivo* setting,
7 myc-tagged WT Dymeclin was used in immunoprecipitation experiments with FLAG-
8 tagged PPIB and GOLM1. Subsequent immunoblotting revealed co-precipitation of both
9 proteins with Dymeclin. In control experiments, lysates from cells transfected with myc-
10 Dymeclin and empty FLAG vector did not show the presence of bands pertaining to PPIB
11 and GOLM1 (Fig. 6B). Additionally, the specificity of the interaction with these proteins
12 was indicated by the inability of Dymeclin to bind the randomly chosen mitochondrial
13 protein, SOD2 (data not shown).
14
15
16
17
18
19
20
21
22
23
24
25
26
27
28

29 **Co-localisation of full-length Dymeclin and PPIB in HeLa cells**

30 The sub-cellular localisation of myc-Dymeclin and PPIB in HeLa cells was examined by
31 indirect immunofluorescence using antibodies against the myc tag and native PPIB.
32 When expressed alone PPIB was dispersed throughout the cytoplasm while Dymeclin, as
33 previously described, was cytosolic with punctate Golgi staining. However, when co-
34 expressed, PPIB co-localised with Dymeclin and displayed a perinuclear distribution,
35 likely aggregating within Golgi and/or ER structures (Fig. 6C). As GOLM1 has long
36 been established to localise to the same cis-Golgi structures as Dymeclin, these data were
37 not replicated in this study [Bachert et al., 2007].
38
39
40
41
42
43
44
45
46
47
48
49
50
51
52
53
54
55
56
57
58
59
60

DISCUSSION

To address the physiological role of Dymeclin and mechanistic basis of DMC disease precipitation and progression, this report utilised a combined approach employing molecular, imaging, proteomic and model system studies.

We utilised a resource of three human DMC fibroblast cell lines to elucidate the effects of Dymeclin mutation on organelle morphology. The cell lines were first characterised at the genomic and transcript level for *DYM* mutations. The splice junction mutations detected in patient lines resulted in heterogeneous consequences for the transcript; in one case both in-frame intronic retention and exonic skipping resulting in premature truncation. However, quantitative PCR performed on all available lines demonstrated a profound loss of *DYM* mRNA, thus indicating that insignificant levels of translational product was likely to be generated in our patient series.

Deleted: significant

Deleted: little if any abnormal translational product was likely to be generated in our patient series

In this study, we have reliably demonstrated *in vitro* that Dymeclin is indeed highly concentrated in the Golgi apparatus but also present in the cytosol. These observations are in accordance with recent publications and suggest that Dymeclin is a peripheral non-anchored Golgi protein capable of shuttling between cellular compartments [Osipovich et al., 2008; Dimitrov et al., 2009]. Immunofluorescence analysis of various cellular compartments emphasised the critical importance of Dymeclin to Golgi structure. In all cell lines analysed, Golgi disorganisation was the most prominent pathogenic feature. Restoration of Golgi structure and juxta-nuclear positioning in patient lines by the over-expression of wild-type protein is a compelling indication that Dymeclin may be

1
2 functionally related to families of structural Golgi proteins including the SNAREs and
3 GRASPs that act in Golgi ribbon formation and/or tethering [Shorter and Warren, 1999;
4 Shorter et al., 1999; Wang et al., 2003]. The developing skeleton has been shown to be
5 particularly affected by mutations in genes disrupting protein secretion and Golgi
6 structure. Electron microscopic analysis of patient fibroblasts noted a marked loss of
7 collagen fibrils surrounding the cell [Nakamura et al., 1997; El Ghouzzi et al., 2003].

Deleted: Electron microscopic analysis of patient fibroblasts confirmed previous observations of an enlarged ER and abnormally high vacuolation but, importantly, we noted a marked loss of collagen fibrils surrounding the cell.

8 This would suggest impairment in the formation of the extracellular matrix, fundamental
9 for chondrogenesis and bone development.

10
11 Patient cells displayed normal rates of proliferation and under standard culture conditions
12 apoptosis also appeared unaffected. However, DMC cells apoptosed at a significantly
13 higher level than WT controls when the process was forced. This finding would suggest
14 that cells lacking Dymeclin are intrinsically more fragile and cell death more likely to
15 occur when the micro-environment is challenged.

16
17
18
19
20
21 By contrast to the mouse and human, embryogenesis in zebrafish can be monitored from
22 the earliest stages as embryos develop outside the mother's body [Kimmel et al., 1995].
23 We studied temporal *dym* expression in this developmental system from the pre-blastula
24 stage to full embryo formation (48 hpf). *Dym*, detected as both a maternal supply and, at
25 the blastula stage, as a zygotic transcript was highly expressed throughout embryogenesis
26 indicating the likely requirement of the protein to embryological developmental
27 processes. Embryonic spatio-temporal expression of *dym*, examined by whole-mount *in*
28 *situ* hybridisation of zebrafish embryos, revealed high levels of the transcript in the
29
30
31
32
33
34
35
36
37
38
39
40
41
42
43
44
45
46
47
48
49
50
51
52
53
54
55
56
57
58
59
60

1
2
3 developing brain and cartilage structures, closely correlating with the key sites of disease
4 in DMC.
5
6
7

8 Both *in vitro* and *in vivo* GOLM1 and PPIB displayed high affinity for Dymeclin.
9
10 GOLM1, a protein of unclear function, stably localises to the cis-Golgi under steady-state
11 conditions. However, when levels of the serine protease furin are increased, typically by
12 TGF- β ligands, the GOLM1 ectodomain is cleaved and secreted via the trans-Golgi and
13 endosomal network into the cytosol and extracellular space [Bachert et al., 2007]. Under
14 physiological conditions, furin cycles from cell membrane to the trans-Golgi network and
15 is dispersed throughout the cell in stark contrast to *Dym* deficient mouse cells where furin
16 accrues in the Golgi [Nakayama, 1997; Rockwell et al., 2002; Osipovich et al., 2008].
17
18 This abnormal accumulation of furin in DMC cells would result in pathogenically high
19 levels of GOLM1 cleavage and release, albeit with unknown functional consequences.
20
21
22
23
24
25
26
27
28
29

30 PPIB, also known as cyclophilin B, belongs to a highly conserved protein family
31 associated with protein post-translational modification and is resident in the ER of all cell
32 types [Price et al., 1991]. PPIB directly binds procollagen in complex with P3HI and
33 CRTRAP and directs it to the Golgi to promote biosynthesis of the mature protein [Price
34 et al., 1991]. Collagen is a key element in generating the osteoid framework required for
35 bone formation [Riminucci and Bianco, 2003]. PPIB mutations generating null alleles in
36 mouse and human lead to the condition osteogenesis imperfecta, characterised by bone
37 fragility due to osteoporosis, reduced bone mass and growth defects [Choi et al., 2009;
38 van Dijk et al., 2009; Barnes et al., 2010]. Of note, collagen accumulates in the ER of
39
40
41
42
43
44
45
46
47
48
49
50
51
52
53
54
55
56
57
58
59
60

1
2 mutant mouse cells with entry into Golgi significantly delayed. Although collagen is
3 secreted to the cell surface, fibril formation and morphology is abnormal [Choi et al.,
4 2009]. As described here and by others Dymeclin plays a central role in multiple protein
5 trafficking pathways opening up the possibility that Dymeclin provides the link between
6 collagen processing by the PPIB complex and vesicular transport [Osipovich et al.,
7 2008]. The loss of interaction between Dymeclin and PPIB may be the mechanistic basis
8 underlying the paucity of collagen fibres observed on the surface of DMC cells by
9 ultrastructural analysis. When taken together, these data underscore a prominent
10 physiological role for Dymeclin in stabilising the Golgi network for effective protein
11 secretion and, further, implicate the PPIB pathway interaction as potentially key to the
12 pathogenesis of DMC.
13
14
15
16
17
18
19
20
21
22
23
24
25
26

27 Through the use of genetically characterised human patient fibroblast lines, this study
28 establishes Dymeclin as integral to Golgi and extracellular matrix structure and provides
29 novel insights into the cellular basis of DMC, in particular the impact of mutation on
30 apoptosis. Expanding the network of interacting proteins consolidates a central position
31 for Dymeclin in intracellular protein secretion and, additionally, identifies specific
32 pathways that provide insight into both cartilage/bone formation and the molecular
33 mechanisms underlying DMC. These data would imply that the molecular basis of DMC
34 shares a common aetiology with other skeletal dysplasias, for example, X-linked
35 spondyloepiphyseal dysplasia tarda and achondrogenesis type 1A [Gedeon et al., 2001;
36 Smits et al., 2010]. These findings are complemented by zebrafish studies demonstrating
37 early and specific dymeclin expression in neural and cartilage development. Future
38
39
40
41
42
43
44
45
46
47
48
49
50
51
52
53
54
55
56
57
58
59
60

1
2 investigations will now be aimed at further elucidating the functional relationship
3
4 between Dymeclin and identified interactors to further interrogate pathways implicated in
5
6 chondrogenesis and bone development.
7
8
9
10

11 12 **ACKNOWLEDGEMENTS**

13
14 This work was supported by the British Heart Foundation [RG/08/006/25302 to R.C.T.,
15
16 FS/07/036 to R.D.M., FS/06/051 to C.D.). The authors acknowledge financial support
17
18 from the Department of Health via the National Institute for Health Research
19
20 comprehensive Biomedical Research Centre award to Guy's & St Thomas' NHS
21
22 Foundation Trust in partnership with King's College London and King's College
23
24 Hospital NHS Foundation Trust.
25
26
27

28 29 **CONFLICT OF INTEREST STATEMENT**

30
31 None to declare.
32
33
34
35
36

37 38 **REFERENCES**

- 39 Agatep R, Kirkpatrick RD, Parchaliuk DL, Woods RA, Gietz RD. 1998. Transformation
40 of *Saccharomyces cerevisiae* by the lithium acetate/single-stranded carrier
41 DNA/polyethylene glycol (LiAc/ss-DNA/PEG) protocol. Technical Tips Online
42 1:P01525.
43 Bachert C, Fimmel C, Linstedt AD. 2007. Endosomal trafficking and proprotein
44 convertase cleavage of cis Golgi protein GP73 produces marker for hepatocellular
45 carcinoma. *Traffic* 8:1415-1423.
46 Barnes AM, Carter EM, Cabral WA, Weis M, Chang W, Makareeva E, Leikin S, Rotimi
47 CN, Eyre DR, Raggio CL, Marini JC. 2010. Lack of cyclophilin B in osteogenesis
48 imperfecta with normal collagen folding. *N Engl J Med* 362:521-528.
49
50
51
52
53
54
55
56
57
58
59
60

- 1
2 Beighton P. 1990. Dyggve-Melchior-Clausen syndrome. *J Med Genet* 27:512-515.
- 3 Choi JW, Sutor SL, Lindquist L, Evans GL, Madden BJ, Bergen HR, 3rd, Hefferan TE,
4 Yaszemski MJ, Bram RJ. 2009. Severe osteogenesis imperfecta in cyclophilin B-
5 deficient mice. *PLoS Genet* 5:e1000750.
- 6 Cohn DH, Ehtesham N, Krakow D, Unger S, Shanske A, Reinker K, Powell BR, Rimoin
7 DL. 2003. Mental retardation and abnormal skeletal development (Dyggve-
8 Melchior-Clausen dysplasia) due to mutations in a novel, evolutionarily
9 conserved gene. *Am J Hum Genet* 72:419-428.
- 10 Dimitrov A, Paupe V, Gueudry C, Sibarita JB, Raposo G, Vielemeyer O, Gilbert T,
11 Csaba Z, Attie-Bitach T, Cormier-Daire V, Gressens P, Rustin P, Perez F, El
12 Ghouzzi V. 2009. The gene responsible for Dyggve-Melchior-Clausen syndrome
13 encodes a novel peripheral membrane protein dynamically associated with the
14 Golgi apparatus. *Hum Mol Genet* 18:440-453.
- 15 Dyggve HV, Melchior JC, Clausen J. 1962. Morquio-Ullrichs Disease : An Inborn Error
16 of Metabolism? *Arch Dis Child* 37:525-534.
- 17 Ehtesham N, Cantor RM, King LM, Reinker K, Powell BR, Shanske A, Unger S, Rimoin
18 DL, Cohn DH. 2002. Evidence that Smith-McCort dysplasia and Dyggve-
19 Melchior-Clausen dysplasia are allelic disorders that result from mutations in a
20 gene on chromosome 18q12. *Am J Hum Genet* 71:947-951.
- 21 El Ghouzzi V, Dagonneau N, Kinning E, Thauvin-Robinet C, Chemaitilly W, Prost-
22 Squarcioni C, Al-Gazali LI, Verloes A, Le Merrer M, Munnich A, Trembath RC,
23 Cormier-Daire V. 2003. Mutations in a novel gene Dymeclin (FLJ20071) are
24 responsible for Dyggve-Melchior-Clausen syndrome. *Hum Mol Genet* 12:357-
25 364.
- 26 Gedeon AK, Tiller GE, Le Merrer M, Heuertz S, Tranebjaerg L, Chitayat D, Robertson
27 S, Glass IA, Savarirayan R, Cole WG, Rimoin DL, Kousseff BG, Ohashi H, Zabel
28 B, Munnich A, Gecz J, Mulley JC. 2001. The molecular basis of X-linked
29 spondyloepiphyseal dysplasia tarda. *Am J Hum Genet* 68:1386-1397.
- 30 Horton WA, Scott CI. 1982. Dyggve-Melchior-Clausen syndrome. A histochemical study
31 of the growth plate. *J Bone Joint Surg Am* 64:408-415.
- 32 James P, Halladay J, Craig EA. 1996. Genomic libraries and a host strain designed for
33 highly efficient two-hybrid selection in yeast. *Genetics* 144:1425-1436.
- 34 Jowett T, Lettice L. 1994. Whole-mount in situ hybridizations on zebrafish embryos
35 using a mixture of digoxigenin- and fluorescein-labelled probes. *Trends Genet*
36 10:73-4.
- 37 Kimmel CB, Ballard WW, Kimmel SR, Ullmann B, Schilling TF. 1995. Stages of
38 embryonic development of the zebrafish. *Dev Dyn* 203:253-310.
- 39 Nakamura K, Kurokawa T, Nagano A, Nakamura S, Taniguchi K, Hamazaki M. 1997.
40 Dyggve-Melchior-Clausen syndrome without mental retardation (Smith-McCort
41 dysplasia): morphological findings in the growth plate of the iliac crest. *Am J*
42 *Med Genet* 72:11-17.
- 43 Nakayama K. 1997. Furin: a mammalian subtilisin/Kex2p-like endoprotease involved in
44 processing of a wide variety of precursor proteins. *Biochem J* 327 (Pt 3):625-635.
- 45 Ortega N, Behonick DJ, Werb Z. 2004. Matrix remodeling during endochondral
46 ossification. *Trends Cell Biol* 14:86-93.
- 47
48
49
50
51
52
53
54
55
56
57
58
59
60

- 1
2
3 Osipovich AB, Jennings JL, Lin Q, Link AJ, Ruley HE. 2008. Dyggve-Melchior-Clausen
4 syndrome: chondrodysplasia resulting from defects in intracellular vesicle traffic.
5 Proc Natl Acad Sci U S A 105:16171-16176.
6 Price ER, Zydowsky LD, Jin MJ, Baker CH, McKeon FD, Walsh CT. 1991. Human
7 cyclophilin B: a second cyclophilin gene encodes a peptidyl-prolyl isomerase with
8 a signal sequence. Proc Natl Acad Sci U S A 88:1903-1907.
9 Riminucci M, Bianco P. 2003. Building bone tissue: matrices and scaffolds in physiology
10 and biotechnology. Braz J Med Biol Res 36:1027-1036.
11 Rockwell NC, Krysan DJ, Komiyama T, Fuller RS. 2002. Precursor processing by
12 kex2/furin proteases. Chem Rev 102:4525-4548.
13 Shorter J, Warren G. 1999. A role for the vesicle tethering protein, p115, in the post-
14 mitotic stacking of reassembling Golgi cisternae in a cell-free system. J Cell Biol
15 146:57-70.
16 Shorter J, Watson R, Giannakou ME, Clarke M, Warren G, Barr FA. 1999. GRASP55, a
17 second mammalian GRASP protein involved in the stacking of Golgi cisternae in
18 a cell-free system. EMBO J 18:4949-4960.
19 Smits P, Bolton AD, Funari V, Hong M, Boyden ED, Lu L, Manning DK, Dwyer ND,
20 Moran JL, Prysak M, Merriman B, Nelson SF, Bonafe L, Superti-Furga A,
21 Ikegawa S, Krakow D, Cohn DH, Kirchhausen T, Warman ML, Beier DR. 2010.
22 Lethal skeletal dysplasia in mice and humans lacking the golgin GMAP-210. N
23 Engl J Med 362:206-216.
24 Spranger J, Maroteaux P, Der Kaloustian VM. 1975. The Dyggve-Melchior-Clausen
25 syndrome. Radiology 114:415-421.
26 Stoll C, Dott B, Roth MP, Alembik Y. 1989. Birth prevalence rates of skeletal dysplasias.
27 Clin Genet 35:88-92.
28 Superti-Furga A, Unger S. 2007. Nosology and classification of genetic skeletal
29 disorders: 2006 revision. Am J Med Genet A 143:1-18.
30 Tannock IF, Lee C. 2001. Evidence against apoptosis as a major mechanism for
31 reproductive cell death following treatment of cell lines with anti-cancer drugs. Br
32 J Cancer 84:100-5.
33 Toledo SP, Saldanha PH, Lamego C, Mourao PA, Dietrich CP, Mattar E. 1979. Dyggve-
34 Melchior-Clausen syndrome: genetic studies and report of affected sibs. Am J
35 Med Genet 4:255-261.
36 van Dijk FS, Nesbitt IM, Zwikstra EH, Nikkels PG, Piersma SR, Fratantoni SA, Jimenez
37 CR, Huizer M, Morsman AC, Cobben JM, van Roij MH, Elting MW, Verbeke JI,
38 Wijnaendts LC, Shaw NJ, Hogler W, McKeown C, Sistermans EA, Dalton A,
39 Meijers-Heijboer H, Pals G. 2009. PPIB mutations cause severe osteogenesis
40 imperfecta. Am J Hum Genet 85:521-527.
41 Wang Y, Seemann J, Pypaert M, Shorter J, Warren G. 2003. A direct role for GRASP65
42 as a mitotically regulated Golgi stacking factor. EMBO J 22:3279-3290.
43
44
45
46
47
48
49
50
51
52
53
54
55
56
57
58
59
60

LEGENDS TO FIGURES

Figure 1. Genetic analysis of DMC fibroblast cell lines. **(A)** Chromatograms of genomic mutations identified in the three DMC lines, altered bases are indicated by arrows and base deletion by a triangle. **(B)** Effect of the splice junction mutations was examined by RT-PCR and gel electrophoresis. The expected PCR products in WT controls and those observed in the mutant samples are marked. Filled arrowheads show the two splice isoforms observed in DMC04997. In each case, aberrant products were gel excised and sequenced to determine the effect of mutations on the transcript. Chromatograms of WT controls are displayed to the left. **(C)** Levels of *DYM* transcript measured by quantitative RT-PCR show greatly reduced expression in all mutants by comparison to the WT control fibroblast line. Measurements were standardised against the housekeeping gene cyclophilin A. Identified mutations in DMC patient samples were numbered at the nucleotide level on the basis that +1 corresponded to the A of the ATG translation initiation codon in the reference sequence.

Figure 2. Dymeclin localises to the cytosol and Golgi. **(A)** Focal co-localization is observed with Giantin (red), a component of the Golgi apparatus, 24 hrs post-transfection of GFP-Dymeclin (green). White arrows indicate areas of overlapping fluorescence. **(B)** By contrast, GFP-Dymeclin (green) displays no evidence for co-localization with the ER marker PDI (red).

Figure 3. Morphological consequences of Dymeclin loss-of-function. **(A)** The Golgi and ER in wild-type (WT) fibroblasts and three patient lines were visualised by Giantin (red)

1
2 and PDI (green) immunofluorescence. Mutant cells display considerably distended Golgi
3
4 by comparison to WT. (B) Electron micrographs of DMC04497 fibroblasts reveal a
5
6 depletion of collagen fibres on the cell surface relative to WT cells as indicated by the
7
8 black arrows. Nuclei are labelled (N). (C) Proliferation assays show no statistical
9
10 difference in proliferation capacity between mutant and WT fibroblasts over an 8 day
11
12 period ($p=0.6610$). FACS analysis of Annexin V stained cells following induced
13
14 apoptosis demonstrate significantly larger populations of mutant cells undergoing
15
16 apoptosis.
17

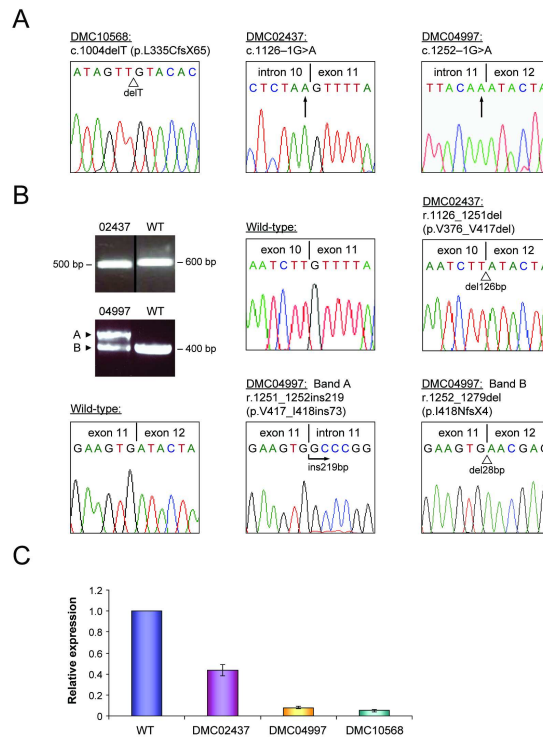
18
19
20 **Figure 4.** Over-expression of Dymeclin leads to Golgi compaction. (A) Comparative to
21
22 fibroblasts transfected with empty GFP vector increasing amounts of WT GFP-Dymeclin
23
24 ($0.5\mu\text{g} - 2\mu\text{g}$) cause condensation of the Golgi, stained with Giantin (red). Golgi position
25
26 in transfected cells is indicated by the white arrows. (B) WT GFP-Dymeclin transfected
27
28 into DMC lines leads to progressive restoration of Golgi morphology, indicated by the
29
30 white arrows, by comparison to neighbouring untransfected cells, where the Golgi is
31
32 identified by double-headed arrows.
33

34
35
36 **Figure 5.** Dymeclin expression in zebrafish embryos. (A) RNA recovered from labelled
37
38 stages of development was reverse transcribed and used to PCR amplify a 1500 bp
39
40 fragment of the Dymeclin transcript. Expression is consistently high in early development
41
42 but decreases by 2 days post-fertilisation. (B) *In situ* hybridisation reveals intense
43
44 staining throughout the brain and head region at 1, 2 and 3 dpf. In addition, dymeclin
45
46 expression becomes detectable in the neuromast sensory organs (n) as highlighted by the
47
48
49
50
51
52
53
54
55
56
57
58
59
60

1
2 arrows. At 5 dpf, the eyes were removed to facilitate assessment of the cartilaginous
3 structures. The staining becomes more prominent in the cartilage of the head, in
4 particular, ceratohyal (ch), ceratobranchial (cb) and lower jaw (lj) structures. Negative
5 controls using the sense strand of dymeclin are displayed in the far-right panels.
6
7
8
9

10
11
12 **Figure 6.** Validation and localisation of Dymeclin interacting proteins. (A) GST pull-
13 down assays were employed to assess *in vitro* binding between Dymeclin and GST-
14 tagged PPIB and GOLM1. The association of both proteins with Dymeclin is indicated
15 by the presence of radio-labelled Dymeclin on the autoradiograph, by contrast Dymeclin
16 is not pulled-down by the GST alone control (left panel). 10% of *in vitro* translated (IVT)
17 Dymeclin used in the pull-down experiment is shown in the panel to the right. (B) HeLa
18 cells were co-transfected with myc-Dymeclin and FLAG-tagged PPIB and GOLM1.
19 Transfected protein levels were assessed by immunoblotting total lysate with anti-FLAG
20 antibody (left panel). Arrows indicate full-length protein. Immunoprecipitation with anti-
21 myc antibody followed by western blot analysis using antibodies against the FLAG tag
22 revealed co-precipitation of PPIB and GOLM1. No protein bands were observed when
23 empty FLAG vector was co-transfected. The asterisk indicates the presence of the
24 immunoglobulin heavy chain. (C) Endogenous PPIB (red) localisation in singly
25 transfected HeLa cells is cytosolic. Co-transfection with GFP-Dymeclin (green) reveals
26 high levels of overlapping perinuclear staining depicted in the merge image (right panel).
27
28
29
30
31
32
33
34
35
36
37
38
39
40
41
42
43
44
45
46
47
48
49
50
51
52
53
54
55
56
57
58
59
60

Figure 1

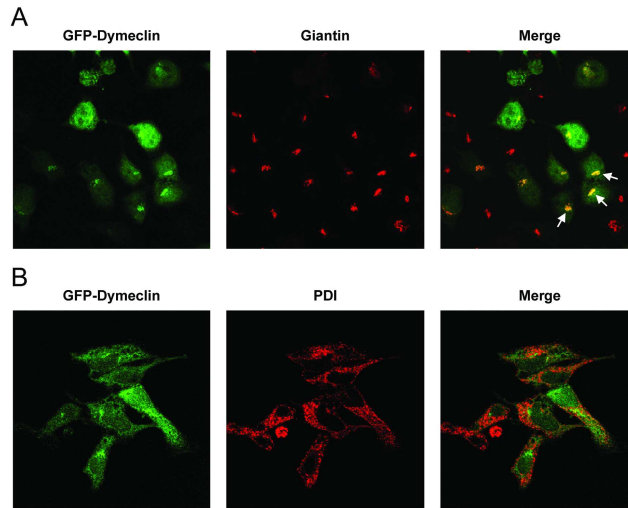


Genetic analysis of DMC fibroblast cell lines. (A) Chromatograms of genomic mutations identified in the three DMC lines, altered bases are indicated by arrows and base deletion by a triangle. (B) Effect of the splice junction mutations was examined by RT-PCR and gel electrophoresis. The expected PCR products in WT controls and those observed in the mutant samples are marked. Filled arrowheads show the two splice isoforms observed in DMC04997. In each case, aberrant products were gel excised and sequenced to determine the effect of mutations on the transcript. Chromatograms of WT controls are displayed to the left. (C) Levels of DYM transcript measured by quantitative RT-PCR show greatly reduced expression in all mutants by comparison to the WT control fibroblast line. Measurements were standardised against the housekeeping gene cyclophilin

A.

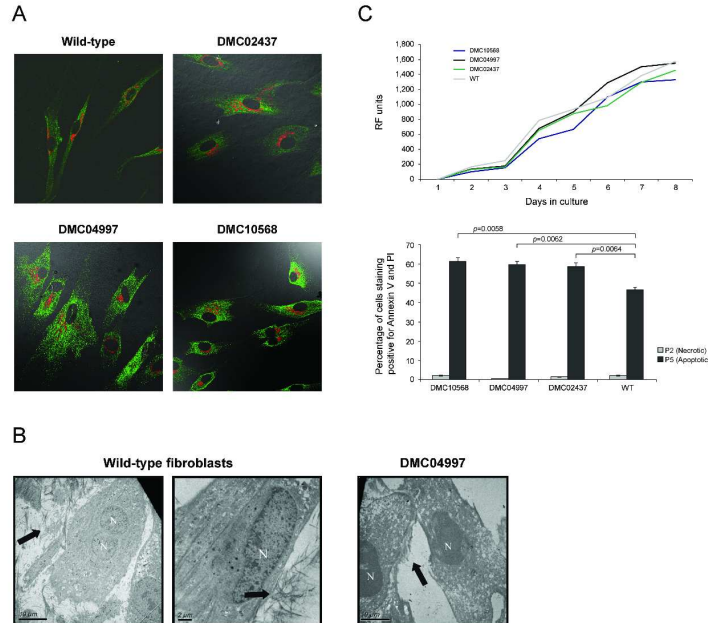
210x297mm (300 x 300 DPI)

Figure 2



Dymeclin localises to the cytosol and Golgi. (A) Focal co-localization is observed with Giantin (red), a component of the Golgi apparatus, 24 hrs post-transfection of GFP-Dymeclin (green). White arrows indicate areas of overlapping fluorescence. (B) By contrast, GFP-Dymeclin (green) displays no evidence for co-localization with the ER marker PDI (red).
210x297mm (300 x 300 DPI)

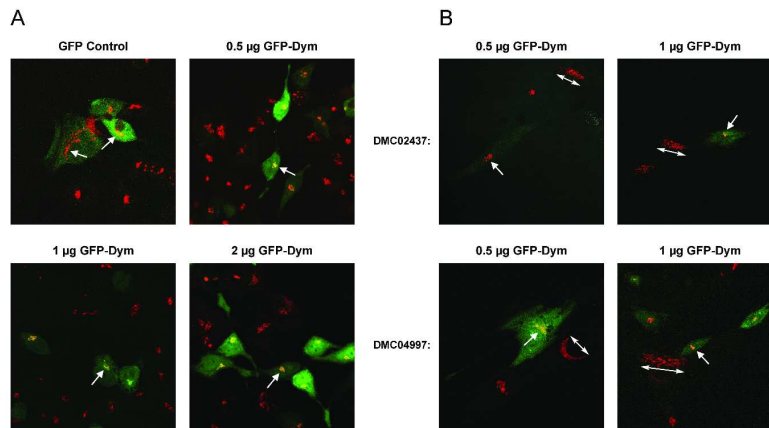
Figure 3



Morphological consequences of Dymeclin loss-of-function. (A) The Golgi and ER in wild-type (WT) fibroblasts and three patient lines were visualised by Giantin (red) and PDI (green) immunofluorescence. Mutant cells display considerably distended Golgi by comparison to WT. (B) Electron micrographs of DMC04497 fibroblasts reveal a depletion of collagen fibres on the cell surface relative to WT cells as indicated by the black arrows. Nuclei are labelled (N). (C) Proliferation assays show no statistical difference in proliferation capacity between mutant and WT fibroblasts over an 8 day period ($p=0.6610$). FACS analysis of Annexin V stained cells following induced apoptosis demonstrate significantly larger populations of mutant cells undergoing apoptosis.

297x210mm (300 x 300 DPI)

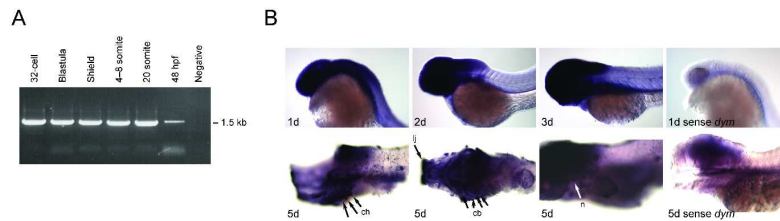
Figure 4



Over-expression of Dymeclin leads to Golgi compaction. (A) Comparative to fibroblasts transfected with empty GFP vector increasing amounts of WT GFP-Dymeclin (0.5µg – 2µg) cause condensation of the Golgi, stained with Giantin (red). Golgi position in transfected cells is indicated by the white arrows. (B) WT GFP-Dymeclin transfected into DMC lines leads to progressive restoration of Golgi morphology, indicated by the white arrows, by comparison to neighbouring untransfected cells, where the Golgi is identified by double-headed arrows.

297x210mm (300 x 300 DPI)

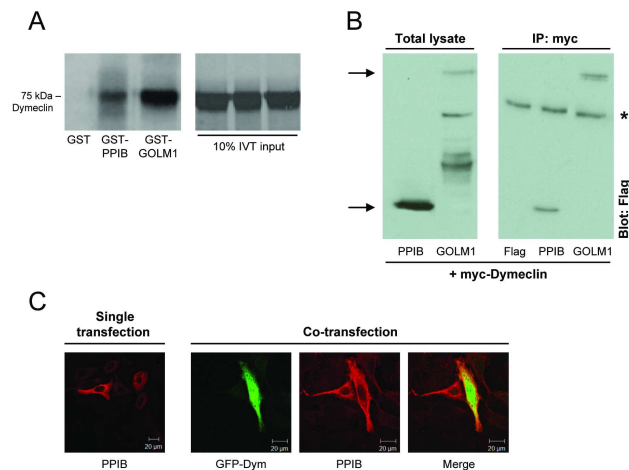
Figure 5



Dymeclin expression in zebrafish embryos. (A) RNA recovered from labelled stages of development was reverse transcribed and used to PCR amplify a 1500 bp fragment of the Dymeclin transcript. Expression is consistently high in early development but decreases by 2 days post-fertilisation. (B) In situ hybridisation reveals intense staining throughout the brain and head region at 1, 2 and 3 dpf. In addition, dymeclin expression becomes detectable in the neuromast sensory organs (n) as highlighted by the arrows. At 5 dpf, the eyes were removed to facilitate assessment of the cartilaginous structures. The staining becomes more prominent in the cartilage of the head, in particular, ceratohyal (ch), ceratobranchial (cb) and lower jaw (lj) structures. Negative controls using the sense strand of dymeclin are displayed in the far-right panels.

297x210mm (300 x 300 DPI)

Figure 6



Validation and localisation of Dymeclin interacting proteins. (A) GST pull-down assays were employed to assess *in vitro* binding between Dymeclin and GST-tagged PPIB and GOLM1. The association of both proteins with Dymeclin is indicated by the presence of radio-labelled Dymeclin on the autoradiograph, by contrast Dymeclin is not pulled-down by the GST alone control (left panel). 10% of *in vitro* translated (IVT) Dymeclin used in the pull-down experiment is shown in the panel to the right. (B) HeLa cells were co-transfected with myc-Dymeclin and FLAG-tagged PPIB and GOLM1. Transfected protein levels were assessed by immunoblotting total lysate with anti-FLAG antibody (left panel). Arrows indicate full-length protein. Immunoprecipitation with anti-myc antibody followed by western blot analysis using antibodies against the FLAG tag revealed co-precipitation of PPIB and GOLM1. No protein bands were observed when empty FLAG vector was co-transfected. The asterisk indicates the presence of the immunoglobulin heavy chain. (C) Endogenous PPIB (red) localisation in singly transfected HeLa cells is cytosolic. Co-transfection with

1
2
3 GFP-Dymeclin (green) reveals high levels of overlapping perinuclear staining depicted in the merge
4 image (right panel).
5 210x297mm (300 x 300 DPI)
6
7
8
9
10
11
12
13
14
15
16
17
18
19
20
21
22
23
24
25
26
27
28
29
30
31
32
33
34
35
36
37
38
39
40
41
42
43
44
45
46
47
48
49
50
51
52
53
54
55
56
57
58
59
60

For Peer Review

TABLES

Identifier	Gender	Ethnic origin	Consanguinity	Clinical summary
DMC02437	Female	Unknown	Unknown	DMC diagnosis with no additional information
DMC04997	Male	Lebanon	Yes	Mental retardation Dwarfism
DMC10568	Male	Pakistan	Yes	Mental retardation Mottled iliac crests Dwarfism

Table 1. Clinical characteristics of DMC subjects.